Available at
http://pvamu.edu/aam
Appl. Appl. Math.
ISSN: 1932-9466

Applications and
Applied Mathematics:
An International Journal
(AAM)

Vol. 10, Issue 2 (December 2015), pp. 893-908

Hydromagnetic Flow and Heat Transfer of Eyring-Powell Fluid over an Oscillatory Stretching Sheet with Thermal Radiation

S. U. Khan and N. Ali
[1] Department of Mathematics and Statistics,
International Islamic University
Islamabad 44000, Pakistan
sk_iiu@yahoo.com
nasirali_qau@yahoo.com

Z. Abbas
Department of Mathematics,
The Islamia University of Bahawalpur,
Bahawalpur 63100, Pakistan
za_qau@yahoo.com

Received: January 28, 2015; Accepted: June 2, 2015

Abstract

An analysis is carried out to investigate the magnetohydrodynamic flow and heat transfer in an unsteady flow of Eyring-Powell fluid over an oscillatory stretching surface. The radiation effects are also considered in energy equation. The flow is induced due to infinite elastic sheet which is stretched periodically back and forth in its own plane. Finite difference scheme is used to solve dimensionless partial differential equations. The effects of emerging parameters on both velocity and temperature profiles are illustrated through graphs. The results obtained by means of finite difference scheme are compared with earlier studies and found in excellent agreement.

Keywords: Boundary layer flow, non-Newtonian fluid, Eyring-Powell fluid, heat flow, oscillatory stretching sheet, finite difference method

MSC 2010 No.: 76A05, 76M20, 76N20

1. Introduction

The boundary layer flow and heat transfer of non-Newtonian fluids over a stretching sheet has numerous applications in various engineering and industrial processes. Such applications include manufacturing of plastic fluids, artificial fibers and polymeric sheets, plastic foam processing,

crystal growing, cooling of metallic sheets in a cooling bath, extrusion of polymer sheet from a die, heat treated materials travelling between a feed role and many others. Besides this, radiation plays a vital role in controlling the heat transfer in the polymer processing industry. In view of all these applications many authors studied the flow of different fluid models over stretching sheet. Sakiadis (1961) initiated the study of boundary layer flow over a flat surface moving with a constant velocity. Since then many researchers extended the work of Sakiadis (1961) for both Newtonian and non-Newtonian fluids. Crane (1970) obtained the closed form solution for the flow caused by stretching of an elastic flat sheet that moves in its own plane. Gupta and Gupta (1977) extended the work of Crane (1970) by considering suction/blowing at the sheet surface. Anderson et al. (1994) studied the diffusion of chemically reactive species over a moving continuous sheet. Golra et al. (1978) discussed unsteady mass transfer in the boundary over a continuous moving sheet. Rajagopal et al. (1984) discussed the flow of viscoelastic second grade fluid over stretching sheet. Pop (1996) studied the unsteady flow past a stretching sheet. Cortell et al. (2006) investigated the heat transfer in an incompressible second grade fluid past a stretching sheet. Ariel (2001) analyzed an axisymmetric flow of second grade fluid past over a radially stretching sheet by finding exact numerical solution. Akyildiz et al (2006) studied the diffusion of chemically reactive species of a non-Newtonian fluid immersed in a porous medium over a stretching sheet. Hayat and Sajid (2007) extended the problem of Ariel (2001) by performing heat transfer analysis with help of homotopy analysis method. Some more contributions in this regard are made by Hayat et al. (2008), Sajid et al. (2012), Nazar et al. (2004), Ishake (2008), Ariel et al. (2006), Nazar et al. (2004), Nandeppanavar et al. (2013), Joshi et al. (2010) and many references therein.

The literature shows that all these investigations are carried out for the case when sheet is only stretched. However, there may arise situations where the sheet is stretched as well as oscillates simultaneously in its own plane. To the best of our knowledge, Wang (1988) was the first who discussed viscous flow due to oscillatory stretching surface. Siddapa et al. (1995) extended Wang's problem for viscoelastic Walter-B fluid. Later on Abbas et al. (2009) included the effects of heat transfer and slip effects on Wang's problem (1988). In another work, Abbas et. al. (2008) reported the hydromagnetic flow of viscoelastic second grade fluid over an oscillatory stretching sheet. Zheng et al. (2013) discussed the Soret and Dufour effects on two-dimensional flow of viscous fluid over a moving oscillatory stretching surface by using homotopy analysis method. Recently Ali et al. (2015) investigated hydromagnetic flow and heat transfer of a Jeffrey fluid over an oscillatory stretching sheet by using homotopy analysis method and finite difference scheme. The literature survey indicates that no attempt is available in the literature which deals with flow and heat transfer of Eyring-Powell fluid over an oscillatory stretching surface with radiation effects.

The purpose of present work is to provide such an analysis. Eyring-Powell fluid model deduced from kinetic theory of liquids rather than the empirical relation (Hayat et al. (2013)). Some studies on flows of Eyring-Powell fluid are reported by Sirohi eta al. (1984), Hayat et al. (2012), Javed et al. (2012) and Hayat (2014).

The structure of this paper is as follows. In Section 2, we present the formulation of the problem. Solution by finite difference method is provided in Section 3. Graphical results obtained through finite difference scheme are shown and discussed in detail in Section 4. Finally, the main conclusions of the study are summarized in Section 5.

2. Flow Analysis

Let us consider an unsteady and two-dimensional flow of incompressible Eyring-Powell fluid over an oscillatory stretching sheet coinciding with plane $\bar{y}=0$ (Figure 1). In the Cartesian coordinate system $\bar{x}$ is along the sheet and $\bar{y}$ is perpendicular to the sheet. Let T_w denote the surface temperature and T_∞ is the temperature of the fluid far away from the surface. It is assumed that $T_w > T_\infty$. A magnetic field of magnitude B_0 is applied in transverse direction to the sheet. Using the boundary layer approximations, continuity, momentum and energy equations are [see Hayat et al. (2014)]

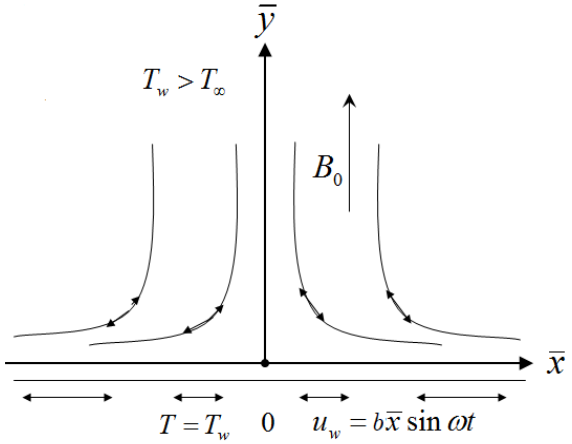

Figure 1. Geometry of the problem

$$\frac{\partial u}{\partial \bar{x}}+\frac{\partial v}{\partial \bar{y}}=0, \tag{1}$$

$$\frac{\partial u}{\partial t}+u\frac{\partial u}{\partial \bar{x}}+v\frac{\partial u}{\partial \bar{y}}=\left(\nu+\frac{1}{\rho\beta C}\right)\frac{\partial^2 u}{\partial \bar{y}^2}-\frac{1}{2\rho\beta C^3}\left[\left(\frac{\partial u}{\partial \bar{y}}\right)^2\frac{\partial^2 u}{\partial \bar{y}^2}\right]-\frac{\sigma B_0^2}{\rho}u, \tag{2}$$

$$\rho c_p\left(\frac{\partial T}{\partial t}+u\frac{\partial T}{\partial \bar{x}}+v\frac{\partial T}{\partial \bar{y}}\right)=k\frac{\partial^2 T}{\partial \bar{y}^2}-\frac{\partial q_r}{\partial \bar{y}}, \tag{3}$$

where u and v are the velocity component along $\bar{x}$ and $\bar{y}$ directions, respectively, ν represents the kinematic viscosity, ρ is the density, β and C are the fluid parameters of the Eyring-Powell model, c_p represents the specific heat, k is the thermal conductivity, σ is the electrical conductivity, T is the temperature and q_r is the radiative heat flux which is given by Rosseland approximation [Raptis et al. (2004)]

$$q_r = -\frac{4\sigma^*}{3k^*}\frac{\partial T^4}{\partial \bar{y}}, \tag{4}$$

where σ^* represents the Stefan Boltzmann constant and k^* is the mean absorption coefficient. Expanding the relation (4) by Tayler series, we get

$$T^4 = T_\infty^4 + 4T_\infty^3\left(T - T_\infty\right) + 6T_\infty^2\left(T - T_\infty\right)^2 + \ldots \tag{5}$$

By neglecting higher-order terms in the above equation, one finds

$$T^4 = 4TT^4 - 3T_\infty^4. \tag{6}$$

In view of (4) and (6), Equation (3) becomes

$$\rho c_p\left(\frac{\partial T}{\partial t} + u\frac{\partial T}{\partial \bar{x}} + v\frac{\partial T}{\partial \bar{y}}\right) = \left(k + \frac{16\sigma^* T_\infty^3}{3k^*}\right)\frac{\partial^2 T}{\partial \bar{y}^2}. \tag{7}$$

The flow is subjected to the following boundary conditions

$$u = u_w = b\bar{x}\sin\omega t, \qquad v = 0, \quad T = Tw \quad \text{at} \quad \bar{y} = 0, \quad t > 0, \tag{8}$$

$$u \to 0, \quad T \to T_\infty \qquad \text{at} \qquad \bar{y} \to \infty, \tag{9}$$

To non-dimensionalize the flow problem, we introduce the following dimensionless variables

$$y = \sqrt{\frac{b}{\nu}}\bar{y}, \quad \tau = t\omega, \quad u = b\bar{x}f_y\left(y,\tau\right), \quad v = -\sqrt{\nu b}\, f\left(y,\tau\right), \tag{10}$$

$$\theta(y,\tau) = \frac{T - T_\infty}{T_w - T_\infty}. \tag{11}$$

In view of the dimensionless variables defined above, the continuity equation is identically satisfied and Equations (2) and (7) reduce to

$$\left(1+K\right)f_{yyy} - Sf_{y\tau} - f_y^2 + ff_{yy} - M^2 f_y - \lambda K f_{yy}^2 f_{yyy} = 0, \tag{12}$$

$$\left(1 + \frac{4}{3}Rd\right)\theta_{yy} + \Pr\left(f\theta_y - S\theta_\tau\right) = 0, \tag{13}$$

with boundary conditions

$$f_y\left(0,\tau\right) = \sin\tau, \qquad f\left(0,\tau\right) = 0, \qquad \theta(0,\tau) = 1, \tag{14}$$

$$f_y\left(\infty,\tau\right) = 0, \qquad \theta(\infty,\tau) = 0. \tag{15}$$

In above equations $K = 1/\mu BC$ and $\lambda = \bar{x}^2 b^3/2\nu C^2$ are dimensionless material fluid

parameters, $S \equiv \omega / b$ is the ratio of the oscillation frequency of the sheet to its stretching rate, $M = \sigma B_0^2 / \rho b$ is the Hartmann number, $\Pr = \mu c_p / k$ is the Prandtl number and $Rd = \dfrac{4\sigma^* T_\infty^3}{kk^*}$ is the radiation parameter**.** According to Javed et al. (2012) equation (12) is subject to the constraint $\lambda K << 1$.

The physical quantities of interest are the skin-friction coefficient C_f and the local Nusselt number Nu_x, which are defined as

$$C_f = \frac{\tau_w}{\rho u_w^2}, \qquad Nu_x = \frac{\bar{x} q_w}{k\left(T_w - T_\infty\right)}, \quad q_w = -k\left(\frac{\partial T}{\partial \bar{y}}\right)_{\bar{y}=0}, \tag{16}$$

where τ_w and q_w are the shear stress and heat flux at wall, respectively. In view of (10) and (11) , Equation (16) takes the following forms

$$\mathrm{Re}_x^{1/2} C_f = (1+K) f_{yy} - \frac{K}{3}\beta\left(f_{yy}\right)_{\bar{y}=0}, \quad \mathrm{Re}_x^{-1/2} Nu_x = -\left(1+\frac{4}{3}Rd\right)\theta_y(0,\tau), \tag{17}$$

where $\mathrm{Re}_x = u_w \bar{x} / \nu$ is the local Reynold number.

3. Direct numerical solution of the problem

We intend to use a finite difference scheme to solve nonlinear boundary value problem consisting of Equations (12) and (13) with boundary conditions (14) and (15). Since, the flow is in unbounded domain, a coordinate transformation $\eta = 1/(y+1)$ is used to transform the semi-infinite physical domain $y \in [0,\infty)$ to finite calculation domain $\eta \in [0,1]$. Thus, we get

$$y = \frac{1}{\eta} - 1, \qquad \frac{\partial}{\partial y} = -\eta^2 \frac{\partial}{\partial \eta}, \qquad \frac{\partial^2}{\partial y^2} = \eta^4 \frac{\partial^2}{\partial \eta^2} + 2\eta^3 \frac{\partial}{\partial \eta}, \qquad \frac{\partial^2}{\partial y \partial \tau} = -\eta^2 \frac{\partial^2}{\partial \eta \partial \tau},$$
$$\frac{\partial^3}{\partial y^3} = -\eta^6 \frac{\partial^3}{\partial \eta^3} - 6\eta^5 \frac{\partial^2}{\partial \eta^2} - 6\eta^4 \frac{\partial}{\partial \eta}.$$

In view of above transformations, Equations (12) and (13) become

$$S\frac{\partial^2 f}{\partial \eta \partial \tau} = \eta^2\left(\frac{\partial f}{\partial \eta}\right)^2 + \left[6(1+K)\eta^2 - 2\eta f\right]\left(\frac{\partial f}{\partial \eta}\right) + \left[6(1+K)\eta^3 - \eta^2 f\right]\left(\frac{\partial^2 f}{\partial \eta^2}\right) + (1+K)\eta^4\left(\frac{\partial^3 f}{\partial \eta^3}\right)$$
$$- M^2\left(\frac{\partial f}{\partial \eta}\right) - \lambda K \eta^{12}\left(\frac{\partial^2 f}{\partial \eta^2}\right)^2\left(\frac{\partial^3 f}{\partial \eta^3}\right) - 6\lambda K \eta^{11}\left(\frac{\partial^2 f}{\partial \eta^2}\right)^3 - 6\lambda K \eta^{10}\left(\frac{\partial f}{\partial \eta}\right)\left(\frac{\partial^2 f}{\partial \eta^2}\right)^2$$

$$-4\lambda K\eta^{10}\left(\frac{\partial f}{\partial \eta}\right)^2\left(\frac{\partial^3 f}{\partial \eta^3}\right)-24\lambda K\eta^{9}\left(\frac{\partial f}{\partial \eta}\right)^2\left(\frac{\partial^2 f}{\partial \eta^2}\right)-24\lambda K\eta^{8}\left(\frac{\partial f}{\partial \eta}\right)^3$$
$$-4\lambda K\eta^{11}\left(\frac{\partial f}{\partial \eta}\right)\left(\frac{\partial^2 f}{\partial \eta^2}\right)\left(\frac{\partial^3 f}{\partial \eta^3}\right)-24\lambda K\eta^{10}\left(\frac{\partial f}{\partial \eta}\right)\left(\frac{\partial^2 f}{\partial \eta^2}\right)^2-24\lambda K\eta^{9}\left(\frac{\partial f}{\partial \eta}\right)^2\left(\frac{\partial^2 f}{\partial \eta^2}\right) \tag{18}$$

$$\left(1+\frac{4}{3}Rd\right)\left(\eta^4\frac{\partial^2\theta}{\partial\eta^2}+2\eta^3\frac{\partial\theta}{\partial\eta}\right)-\Pr\left(f\eta^2\frac{\partial\theta}{\partial\eta}+S\frac{\partial\theta}{\partial\tau}\right)=0, \tag{19}$$

$$\frac{\partial f}{\partial\eta}=0,\qquad \theta=0 \quad \text{at} \quad \eta=0, \tag{20}$$

$$f=0,\quad \frac{\partial f}{\partial\eta}=-\sin\tau,\quad \theta=1 \ \text{ at } \ \eta=1. \tag{21}$$

Equations (18) and (19) are discretized for L uniformly distributed discrete points $\left(\eta_1,\ \eta_2,...,\ \eta_{\{L\}}\right)\in\left(0,\ 1\right)$ with a space grid size of $\Delta\eta=1/\left(L+1\right)$ and time level $t=\left(t^1,\ t^2,...\right)$. Hence the discrete values $\left(f_1^n,\ f_2^n,\ ...,\ f_L^n\right)$ and $\left(\theta_1^n,\ \theta_2^n,\ ...,\ \theta_L^n\right)$ at these grid point for time levels $t^n=n\Delta t$ $\left(\Delta t \text{ is the time step}\right)$ can be numerically solved together with boundary conditions at $\eta=\eta_0=0$ and $\eta=\eta_{\{L+1\}}=1$. We start our simulations from a motionless velocity field and a uniform temperature distribution equal to temperature at infinity as

$$f\left(\eta,\tau=0\right)=0 \quad \text{and} \quad \theta\left(\eta,\tau=0\right)=0. \tag{22}$$

Following Abbas et al. (2009) an implicit difference scheme is constructed for velocity f and temperature θ as follows

$$S\frac{1}{\Delta t}\left(\frac{\partial f^{(n+1)}}{\partial\eta}-\frac{\partial f^{(n)}}{\partial\eta}\right)=\eta^2\left(\frac{\partial f^{(n)}}{\partial\eta}\right)^2+\left[6\left(1+K\right)\eta^2\right]\left(\frac{\partial f^{(n+1)}}{\partial\eta}\right)-2\eta f^{(n)}\left(\frac{\partial f^{(n)}}{\partial\eta}\right)$$
$$+6\left(1+K\right)\eta^3\left(\frac{\partial^2 f^{(n+1)}}{\partial\eta^2}\right)-2\eta f^{(n)}\left(\frac{\partial f^{(n)}}{\partial\eta}\right)-\eta^2 f^{(n)}\left(\frac{\partial^2 f^{(n)}}{\partial\eta^2}\right)$$
$$+\left(1+K\right)\eta^4\left(\frac{\partial^3 f^{(n+1)}}{\partial\eta^3}\right)-M^2\left(\frac{\partial f^{(n+1)}}{\partial\eta}\right)-\lambda K\eta^{12}\left(\frac{\partial^2 f^{(n)}}{\partial\eta^2}\right)^2\left(\frac{\partial^3 f^{(n)}}{\partial\eta^3}\right)$$
$$-6\lambda K\eta^{11}\left(\frac{\partial^2 f^{(n)}}{\partial\eta^2}\right)^3-6\lambda K\eta^{10}\left(\frac{\partial f^{(n)}}{\partial\eta}\right)\left(\frac{\partial^2 f^{(n)}}{\partial\eta^2}\right)^2$$

$$-4\lambda K\eta^{10}\left(\frac{\partial f^{(n)}}{\partial \eta}\right)^2\left(\frac{\partial^3 f^{(n)}}{\partial \eta^3}\right)-24\lambda K\eta^{9}\left(\frac{\partial f^{(n)}}{\partial \eta}\right)^2\left(\frac{\partial^2 f^{(n)}}{\partial \eta^2}\right)$$

$$-24\lambda K\eta^{8}\left(\frac{\partial f^{(n)}}{\partial \eta}\right)^3-4\lambda K\eta^{11}\left(\frac{\partial f^{(n)}}{\partial \eta}\right)\left(\frac{\partial^2 f^{(n)}}{\partial \eta^2}\right)\left(\frac{\partial^3 f^{(n)}}{\partial \eta^3}\right)$$

$$-24\lambda K\eta^{10}\left(\frac{\partial f^{(n)}}{\partial \eta}\right)\left(\frac{\partial^2 f^{(n)}}{\partial \eta^2}\right)^2-24\lambda K\eta^{9}\left(\frac{\partial f^{(n)}}{\partial \eta}\right)^2\left(\frac{\partial^2 f^{(n)}}{\partial \eta^2}\right) \tag{23}$$

$$S\,\mathrm{Pr}\frac{\left(\theta^{(n+1)}-\theta^{(n)}\right)}{\Delta t}=\left(1+\frac{4}{3}Rd\right)\left(\eta^4\frac{\partial^2\theta^{(n+1)}}{\partial\eta^2}+2\eta^3\frac{\partial\theta^{(n+1)}}{\partial\eta}\right)-\mathrm{Pr}\,f^{(n)}\eta^2\frac{\partial\theta^{(n+1)}}{\partial\eta}.$$

In this way, only linear equations at new time step $(n+1)$ are to be solved. It should be noted that other different choices of time differences are also possible. By using finite difference method two systems of linear equations for $f_i^{(n+1)}$ and $\theta_i^{(n+1)}$ $i=(1,\ 2,...,L)$ at the time step $(n+1)$ are obtained which can be solved with help of the Gaussian elimination.

4. Results and discussion

In order to discuss the effects of emerging parameters on velocity and temperature fields, the numerical technique discussed in the previous section is implemented to solve the non-linear partial differential Equations (12) and (13) with boundary conditions (14) and (15). In this section, we discuss the effects of involved parameters graphically. In all the plots, the values of K and λ are chosen so that the product λK should be very sufficiently smaller than unity.

Figure 2 depicts the effects of the relative amplitude of frequency to the stretching rate S, Hartmann number M and fluid parameters λ on the time-series of the velocity component f' at a fixed distance $y=0.25$ from the sheet, respectively. Figure 2(a) shows the effects of the S on the time-series of the velocity profile f' by keeping $K=0.1,\ \lambda=0.1$ and $M=0.5$ fixed. This figure shows that the amplitude of the flow motion decreases by increasing S. Furthermore, one can easily observe that a phase shift occurs which increases for large values S. Figure 2(b) elucidates the behavior of Hartmann number M on the time-series of the velocity component f'. As expected, the amplitude of the flow motion decreases by increasing Hatmann number M. The reason is that magnetic field acts as a resistance to the flow. Figure 2(c) shows that an increase in fluid parameter λ results in an increase of amplitude f'.

Figure 3(a) shows a comparison of transverse profile of velocity f' for Newtonian and Eyring-Powell fluids. It is evident that magnitude of velocity inside the boundary layer for Eyring-Powell fluid is greater than the magnitude of velocity for Newtonian fluid. Similarly amplitude of time-series of f' for Eyring-Powell fluid is also greater than the amplitude of time-series of f' for Newtonian fluid (Figure 3(b)).

Figure 4 shows the influence of relative amplitude of frequency to the stretching rate S on transverse profile of velocity f' at four different time instants $\tau = 8.5\pi$, $\tau = 9\pi$, $\tau = 9.5\pi$ and $\tau = 10\pi$. Figure $4(a)$ is plotted at time instant $\tau = 8.5\pi$. From this figure we see that velocity decreases by increasing S. At time instant $\tau = 9\pi$ (Figure $4(b)$) the velocity f' at the surface is zero and for away from the surface it again approaches zero. Moreover, at this time instant it oscillates near the wall. Figure $4(c)$ shows the effects of S on f' at $\tau = 9.5\pi$. From this Figure we note that velocity decreases from -1 at the surface to zero far away from the surface. The effects of S on f' at time instant $\tau = 10\pi$ are similar to the effects of S on f' at time instant $\tau = 9\pi$.

The variation of Hartmann number M on transverse profile of velocity f' at different time instants $\tau = 8.5\pi$, $\tau = 9\pi$, $\tau = 9.5\pi$ and $\tau = 10\pi$ are shown in Figure 5. Figure $5(a)$ shows that an increase in Hartmann number M causes a decrease in the velocity at time instant $\tau = 8.5\pi$. Furthermore, the boundary layer thickness is also found to decrease. It is observed from Figure 5(b) that at $\tau = 9\pi$, the velocity f' oscillates near the surface and approaches to zero far away from the surface. Figure $5(c)$ shows that at $\tau = 9.5\pi$, the velocity f' at the surface decreases from -1 to zero far away from the surface. Moreover, at this time instant there exists no oscillation in the velocity f'. The velocity profile at time instant $\tau = 10\pi$ is illustrated in Figure $5(d)$. From this Figure one can observe that velocity oscillates near the sheet and approaches zero far away from the surface.

Figure 6 illustrates the influence of fluid parameter λ on the velocity profile f' at four different time instants $\tau = 8.5\pi$, $\tau = 9\pi$, $\tau = 9.5\pi$ and $\tau = 10\pi$. Figure $6(a)$ shows the variation of fluid parameter λ at $\tau = 8.5\pi$. Here, we see the velocity f' increases by increasing fluid parameter λ. From Figure $6(b)$, it can be seen that the velocity oscillates near the sheet before approaching zero far away from the sheet. The effects of λ at time instant $\tau = 9.5\pi$ are illustrated in Figure $6(c)$. An opposite trend is found in velocity at this time instant, i.e. the velocity increases by increasing fluid parameter λ. The behavior of fluid parameter λ at time instant $\tau = 10\pi$ is shown in Figure $6(d)$.

Figure 7 describes the effects of Hartmann number M relative amplitude of frequency to the stretching rate S, fluid parameter K and λ on the time-series of shear stress at the wall for the first five periods $\tau \in [0, 10\pi]$. Figure $7(a)$ shows the influence the variation of Hartmann number M on the skin-friction coefficient $\mathrm{Re}_x^{1/2} C_f$ by keeping other parameters fixed. It is clear from this Figure that the amplitude of oscillation of the skin-friction coefficient increases by increasing Hartmann number M. From Figure 7(b), we observe that skin friction coefficient oscillates with time and the amplitude of oscillation increases for large values of S. The effects of fluid parameter K and λ are shown in Figures $7(c)$ and (d), respectively. In these Figures an opposite trend is observed. These Figures show that the skin friction coefficient $\mathrm{Re}_x^{1/2} C_f$ decreases monotonically by increasing the fluid parameters. The temperature profile θ for different values of S, Pr, Rd and M are shown in Figure 8.

Figure $8(a)$ illustrates that temperature and thermal boundary layer thickness decreases by increasing S. Figure $8(b)$, depicts the influence of Prandtl number $\Pr$ on the temperature field θ by keeping other parameters constant. It can be identified from this Figure that with the increase of Prandtl number $\Pr$ i.e., with decrease of thermal diffusively or the increase of specific heat, the increase in the fluid temperature is relatively slow. The effects of radiation parameter Rd on temperature profile θ are illustrated in Figure $8(c)$. It is clear from the graph that an increase in radiation parameter Rd results in increase of temperature field θ. Figure $8(d)$ is plotted to see the effects of Hartmann number M on the temperature profile θ. As expected, the temperature profile increases by increasing Hartmann number M. We also note that thermal boundary layer thickness increases by increasing Hartmann number M.

Figure 9 is plotted to see the effects of $\Pr$, S and Rd on the time-series of temperature profile θ. Figure $9(a)$ shows the effects of Prandtl number $\Pr$ on the time-series of temperature θ by keeping $K = 0.1,\ Rd = 0.5, M = 5$ and $S = 0.8$. From this Figure it is clear that the temperature decreases for large values of $\Pr$. We also observe small amplitude of oscillations in temperature θ for large of values of $\Pr$. The effect of S are similar to that of $\Pr$ (Figure $9(b)$). Figure $9(c)$ shows an opposite behavior. From this Figure it is clear that time-series of temperature profile increases by increasing radiation parameter. Again, small amplitude oscillations are observed in temperature for all values of radiation parameter Rd.

Table 1 shows the comparison of present study with Zheng et al. (2013). From the table we observe that the present results show an excellent correlation agreement with previous study. The numerical values of local Nusselt number for different values of $\Pr$, λ M , K and Rd are tabulated in Table 2. From this table it is clear that local Nusselt number increases by increasing Prandtl number $\Pr$, radiation parameter Rd and fluid parameter K while it decreases by increases by increasing Hartmann number M and fluid parameter β.

Table 1. Comparison of values of $f''(0,\tau)$ for fluid parameters $K = \lambda = 0$ (Newtonian case) with Zheng.et al. (2013).

$M = 12$	$S = 1$	τ	Zheng et al. (2013)	Present results
12.0	1.0	1.5π	11.678565	11.678656
		5.5π	11.678706	11.678707
		9.5π	11.678656	11.678656

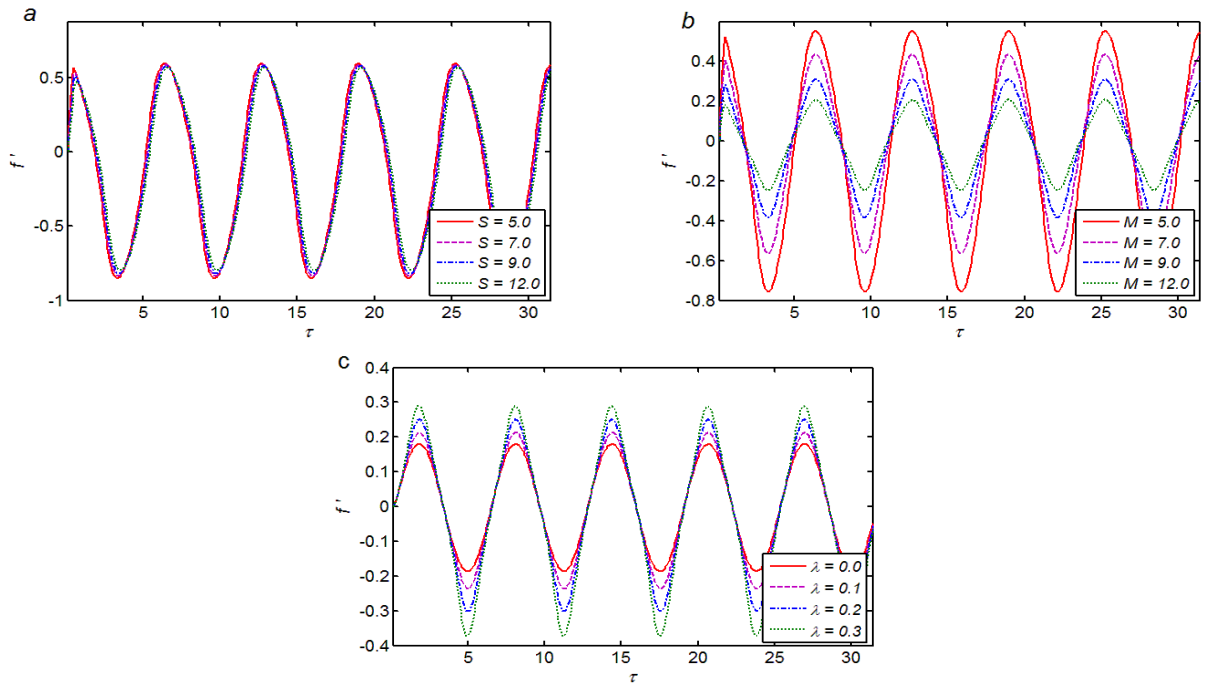

Figure 2. Time-series of the velocity profile f' in the first five periods $\tau \in [0,10\pi]$ at a fixed distance to the sheet, $y = 0.25$: (a) effects of S with, $K = 0.1$, $\lambda = 0.1$ and $M = 0.5$ (b) effects of M with $S = 5$, $K = 0.1$ and $\lambda = 0.1$ and (c) effects of λ with $S = 15$, $K = 0.1$, $M = 5$.

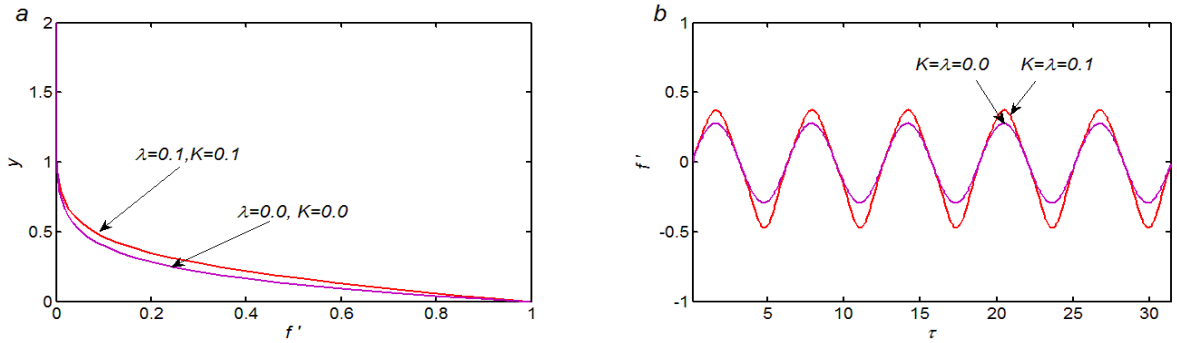

Figure 3. The comparison of Newtonian and non-Newtonian fluids (a) Transverse profile of velocity field (b) Time-series of velocity field with $S = 15$ and $M = 5$.

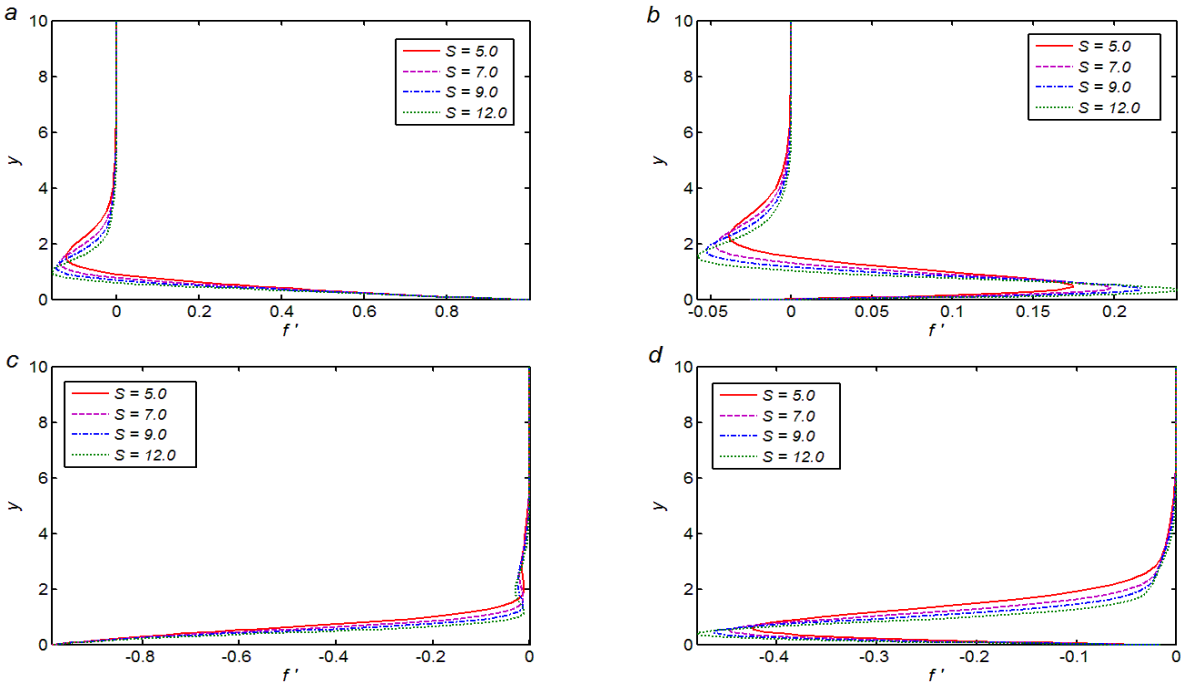

Figure 4. Transverse profiles of the velocity field f' for the different values of S in the fifth period $\tau \in [8\pi, 10\pi]$, (a) $\tau = 8.5\pi$, (b) $\tau = 9\pi$, (c) $\tau = 9.5\pi$, and (d) $\tau = 10\pi$, with $K = 0.1$, $\lambda = 0.1$ and $M = 1.0$.

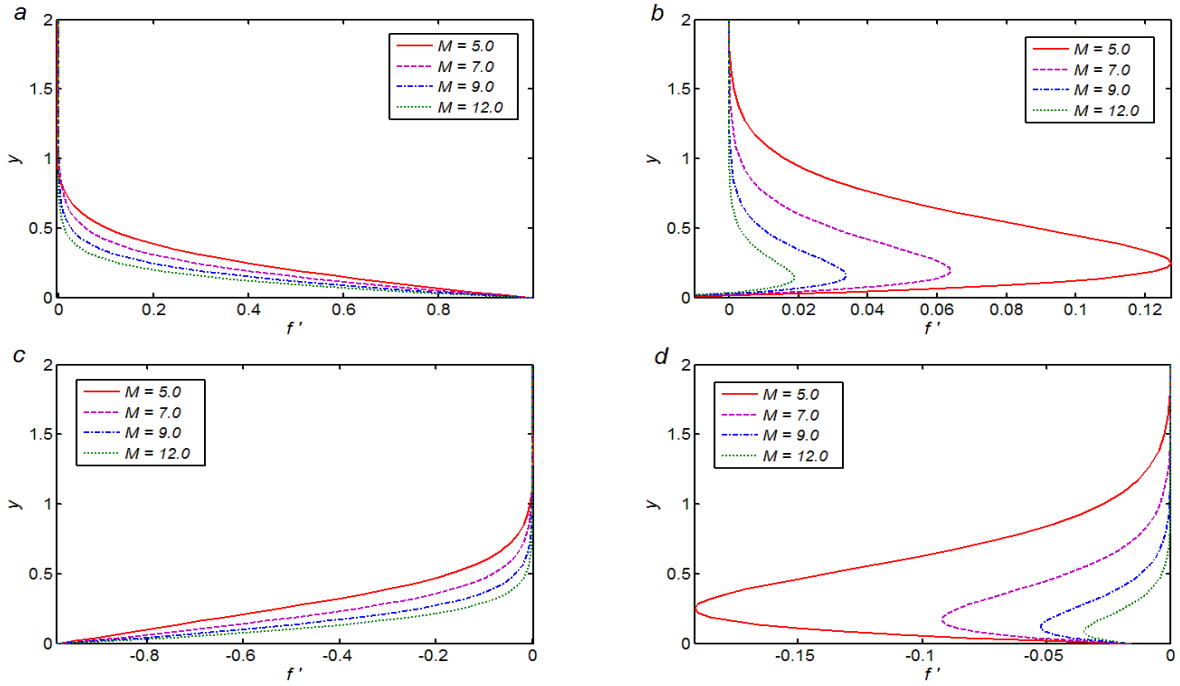

Figure 5. Transverse profiles of the velocity field f' for different values of M in the fifth period $\tau \in [8\pi, 10\pi]$, (a) $\tau = 8.5\pi$, (b) $\tau = 9\pi$, (c) $\tau = 9.5\pi$ and (d) $\tau = 10\pi$ with

$S=15,\ K=0.1$ and $\lambda=0.1.$

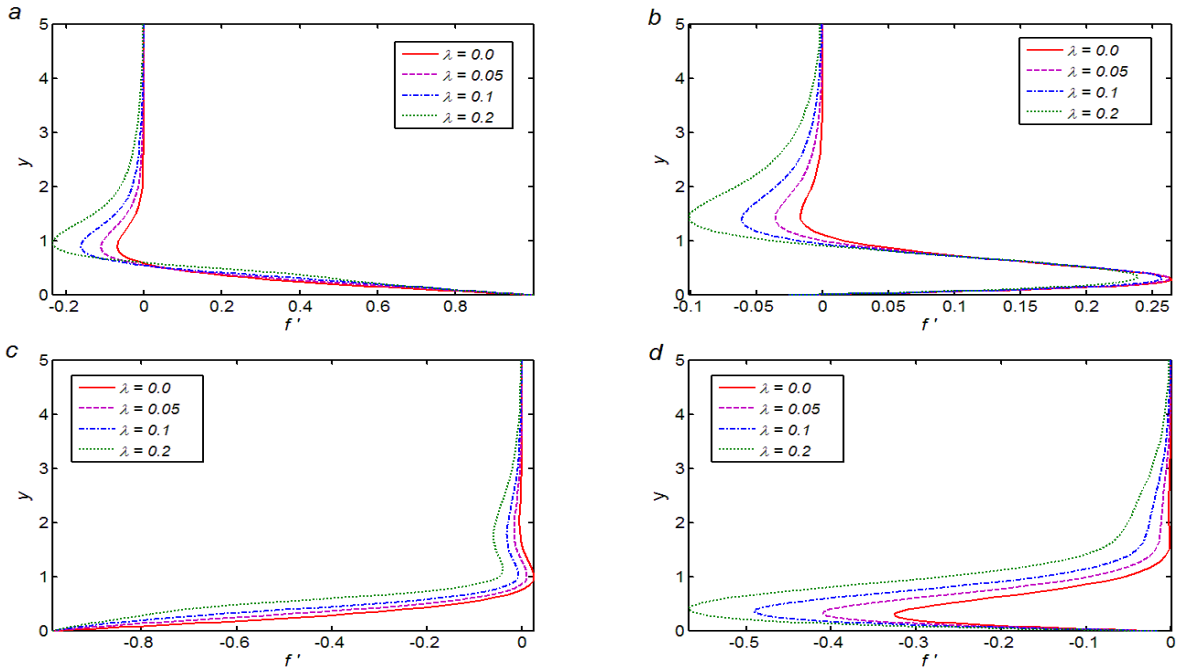

Figure 6. Transverses profile of the velocity field f' for different values of λ in the fifth period $\tau\in[8\pi,10\pi]$, (a) $\tau=8.5\pi$, (b) $\tau=9\pi$, (c) $\tau=9.5\pi$ and (d) $\tau=10\pi$ with $S=15,\ K=0.1$ and $M=1.$

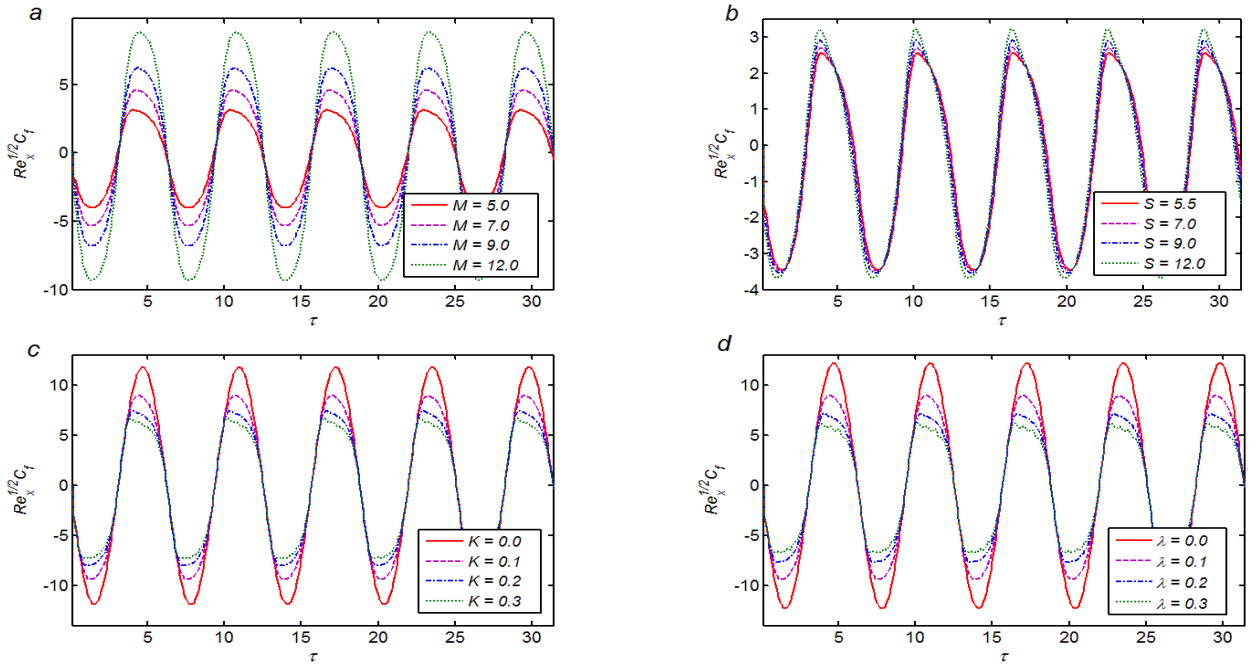

Figure 7. Time-series of the skin friction coefficient in the first five periods $\tau\in[0,10\pi]$ at a fixed distance to the sheet, $y=0.25$: *(a)* effects of M with $S=5,\ \lambda=0.1$ and $K=0.1$ (b) effects of S with $M=4,\ \lambda=0.1$ and $K=0.1$, (c) effects of K with $S=12$, $\lambda=0.1$, $M=12$ and (d) effects of λ with $S=12$, $K=0.1$ and $M=12.$

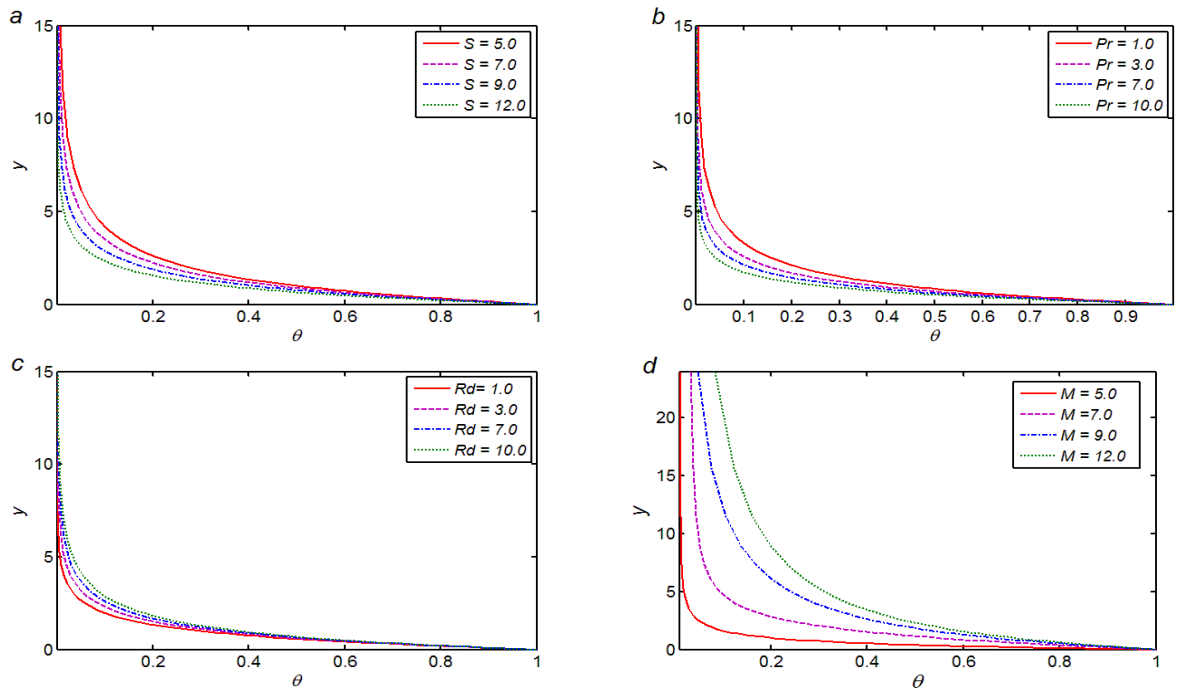

Figure 8. Transverse profiles of the temperature field θ at $\tau = 8\pi$: *(a)* effects of S with $K = 0.1$, $\lambda = 0.1$, $M = 5$, $\Pr = 10$, $Rd = 0.5$, *(b)* effects of $\Pr$ with $K = 0.1$, $\lambda = 0.1$, $M = 5$, $S = 15$, $Rd = 0.5$, (c) effects of Rd of with $K = 0.1$, $\lambda = 0.1$, $M = 5$, $\Pr = 10$ and $S = 15$ (d) effects of M of with $K = 0.1$, $\lambda = 0.1$, $Rd = 5$, $\Pr = 10$ and $S = 15$.

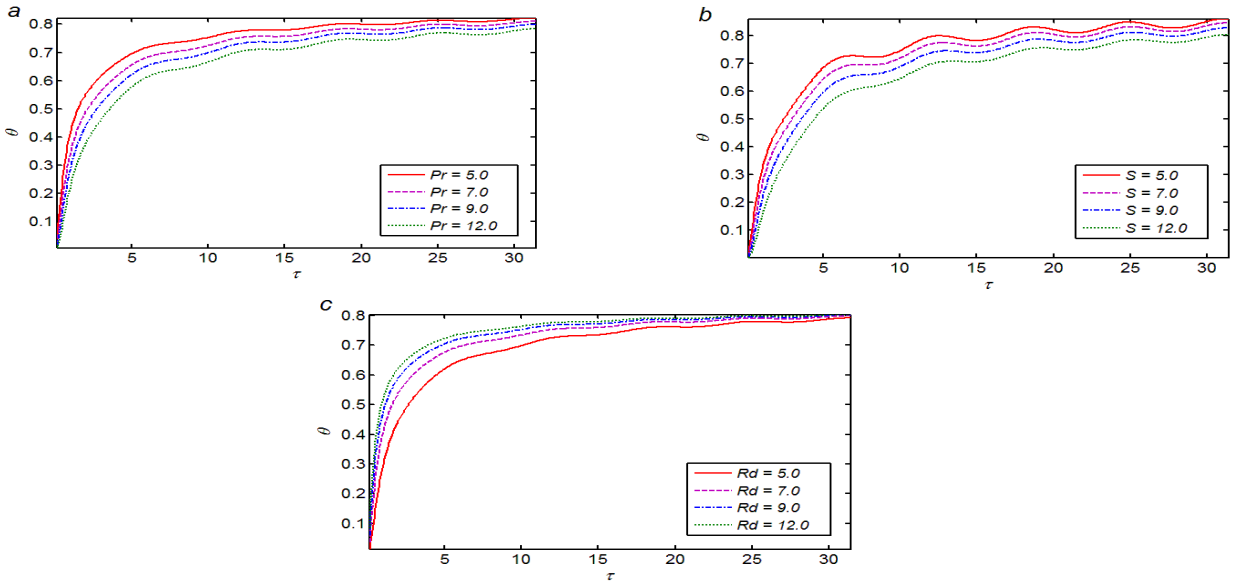

Figure 9. Time-series of the temperature $\theta, \tau \in [0, 10\pi]$ at $y = 0.25$ (a) effects of $\Pr$ with $K = 0.1$, $\lambda = 0.1$, $M = 5$, $S = 0.8$, $Rd = 0.5$, (*b*) effects of S with $K = 0.1$, $\lambda = 0.1$, $M = 5$,*Pr=10*, $Rd = 2.5$ and *(c)* effects of Rd of with $K = 0.1$, $\lambda = 0.1$, $M = 10$, $\Pr = 10$ and $S = 15$.

Table 2. The numerical values of local Nusselt number $-\left(1+\frac{4}{3}Rd\right)\theta'(0,\tau)$ for various values of Prandtl number $\Pr$, radiation parameter Rd, Hartmann number M, fluid parameter λ and K when the ratio of the oscillation frequency of the sheet to its stretching rate $S=0.5$ at time instant $\tau=\pi/2$.

$\Pr$	K	M	Rd	λ	$-\left(1+\frac{4}{3}Rd\right)\theta'(0,\tau)$
1.0	0.5	0.5	0.2	0.5	1.71214
1.5					1.75424
2.0					1.86546
0.2	0.0				1.65745
	0.2				1.74201
	0.4				1.76201
	0.5	0.2			1.65420
		0.4			1.62548
		0.6			1.56421
		0.5	0.0		1.56741
			0.2		1.65846
			0.4		1.76213
			0.2	0.0	1.71234
				0.3	1.71210
				0.6	1.70125

5. Concluding remarks

In this article, we have analyzed the study of an Eyring-Powell fluid over an oscillatory stretching heated sheet in the presence of thermal radiation. A coordinate transformation is used to transform the semi-infinite flow domain to a finite computational domain. A finite difference scheme is used to solve the governing nonlinear partial differential equations. The time-series of the flow velocity, the temperature, the structure of the boundary layer near the plate are illustrated graphically for various values of parameters of interest. The main observations of study are:

- The amplitude of velocity decreases by increasing S, Hartmann number M, and fluid parameter K.
- The temperature increases by increasing Hartmann number M and radiation parameter Rd while it decreases with increase of Prandtl number $\Pr$ and ratio of the oscillation frequency of the sheet to its stretching rate S.
- The local Nusselt number increases by increasing Prandtl number $\Pr$, fluid parameter K, radiation parameter Rd while it decreases by increasing Hartmann number M and fluid parameter λ.

Acknowledgements:

We are thankful to the anonymous reviewer for his/her useful comments to improve the earlier version of the paper.

REFERENCES

Abbas, Z., Wang, Y., Hayat, T. Oberlack, M. (2009). Slip effects and heat transfer analysis in a Viscous fluid over an oscillatory stretching surface. Int. J. Numer. Meth. Fluids, Vol. 59, pp. 443-458

Abbas, Z., Wang, Y., Hayat, T., Oberlack, M. (2008). Hydromagnetic flow in a viscoelastic fluid due to the oscillatory stretching surface, Int. J. Non Lin. Mech. Vol. 43, pp. 783-793.

Akyilidiz, F. T., Bellout, H. and Vajravelu, K. (2006). Diffusion of chemical reactive species in porous medium over a stretching sheet, J Math. Anal. Appl. (2006) pp. 322-339.

Ali, N., Khan, S.U. and Abbas, Z. (2015). Hydromagnetic flow and heat transfer of a Jeffrey-fluid, over an oscillatory stretching surface Z. Naturforsch A. DOI 10.1515/zna-2014-0273 (In Press).

Anderson, H. I., Hansen, O. R. and Olmedal, B. (1994). Diffusion of chemically reactive species from a stretching sheet, Int. J. Heat Mass Transf., Vol. 37, pp. 659-664.

Ariel, P.D. (2001). Axismmetric flow of a second grade fluid past a stretching sheet. Int. J. Eng. Sci. Vol. 39, pp. 529-553.

Ariel, P.D., Hayat, T. and Asghar, S. (2006). The flow of an elastico-viscous fluid past stretching sheet with partial slip, Acta. Mech. Vol. 187, pp. 29-35.

Cortell, R. (2006). A note on flow and heat transfer of viscoelastic fluid over a stretching sheet, Int. J. Non-Lin. Mech. Vol. 41, pp. 78-85.

Crane, L.J. (1970). Flow past a stretching plate. Z Angew Math Phys. (ZAMP), Vol. 21, pp. 645-647.

Gorla, R.S. R. (1978). Unsteady mass transfer in the boundary layer on continuos moving sheet electrode, J. Electrochem. Soc. Vol. 125, pp. 865-869.

Gupta, P. S. and Gupta, A. S. (1977). Heat and mass transfer on stretching sheet with suction or blowing, Can. J. Chem. Eng. Vol. 55, pp. 744-746.

Hayat, T. and Sajid, M. (2007). Analytic solution for axisymmetric flow and heat transfer flow of a second grade fluid past a stretching sheet. Int. J. Heat Mass Transf., Vol. 50, pp. 75-84.

Hayat, T., Abbas, Z. and Sajid, M. (2008). Heat and mass transfer analysis on the flow of second grade fluid in the presence of chemical reaction, Phys. Lett. A, Vol. 372, pp. 2400-2408.

Hayat, T., Asad, S., Mustafa, M. and Alsaedi, A. (2014). Radiation effects on the flow of Powell-Eyring fluid past an unsteady inclined stretching sheet with Non-uniform heat source/sink. PLOS ONE 9(7): e103214. doi:10.1371/journal.pone.0103214.

Hayat, T., Awais, M. and Asghar, S. (2013). Radiative effects in a three-dimensional flow of MHD Eyring-Powell fluid, J. Egyp. Math. Society, Vol. 21, pp. 379-384.

Hayat, T., Iqbal, Z., Qasim, M.and Obaidat, S. (2012). Steady flow of an Eyring Powell fluid over a moving surface with convective boundary conditions, Int. J. Heat Mass Transf. Vol. 55, pp. 1817-1822.

Ishake, A., Nazar, R. and Pop, I. (2008). Mixed convection stagnation point flow towards a stretching sheet, Meccania Vol. 43, pp. 411-418.

Javed, T., Ali, N., Abbas, Z. and Sajid, M. (2012). Flow of an Eyring-Powell non-Newtonian over a stretching sheet, Chem. Eng. Commun., Vol. 200, pp. 327-336

Joshi, N. and Kumar, M. (2010). The Combined Effect of Chemical reaction, Radiation, MHD on Mixed Convection Heat and Mass Transfer Along a Vertical Moving Surface, Appl.

Appl. Math. Vol. 05, Issue 2 (December 2010), pp. 534 – 543.
Nandeppanavar, M. M, Siddalingappa, M. N., Jyoti, H.,(2013). Heat Transfer of viscoelastic fluid flow due to stretching sheet with internal heat source, Int. App. Mech. Eng. Vol. 18, pp.739-760.
Nazar, R., Amin, N., Filip, D. and Pop, I. (2004). Stagnation point flow of a micropolar fluid towards a stretching sheet, Int. J. Non-linear Mech. Vol. 39, pp. 1227-1235.
Nazar, R., Amin, N., Pop, I. (2004). Unsteady boundary layer flow due to stretching surface in a rotating fluid. Mech Res Commun. Vol. 31, pp. 121-128.
Pop, I, Na, T Y. (1996). Unsteady flow past a stretching sheet. Mech. Res. Comm. Vol. 23, pp. 413-422.
Rajagopal, K. R., Na, T. Y. and Gupta, A. S. (1984). Flow of viscoelastic fluid over a stretching sheet, Rheol. Acta. Vol. 31, pp. 213-215.
Raptis, A., Perdikis, C. and Takhar, H. S. (2004). Effect of thermal radiation on MHD flow, Appl. Math. Comput. Vol. 153, pp. 645-649.
Sajid, M., Abbas, Z., Ali, N. and Javed, T. (2012). Stretching a surface having a layer of porous medium in a viscous fluid, Appl. Appl. Math. Vol. 7, pp. 609 - 618.Sakiadis, B.C. (1961). Boundary layer behavior on continuous solid surfaces, AIChE J. Vol. 7, pp. 26-28
Siddappa, B., Abel, S. and Hongunti V. (1995). Oscillatory motion of a viscoelastic fluid past a stretching sheet, ll Nuovo Cimento D Vol. 17, pp. 53.
Sirohi, V., Timol, M.G.and Kalathia, N.L. (1984). Numerical treatment of Powell-Eyring fluid flow past a 90 degree wedge, Reg. J. Energy Heat Mass Transf., Vol. 6, pp. 219-228.
Wang, C. Y. (1988). Nonlinear streaming due to the oscillatory stretching of a sheet in a Viscous, Acta Mech. Vol. 72, pp. 261-268.
Zheng, L.C, Jin, X., Zhang, X. X, Zhang, J. H. (2013). Unsteady heat and mass transfer in MHD flow over an oscillatory stretching surface with Soret and Dufour effects, Acta Mech. Sin., Vol. 29, pp. 667-675.